ACS APPLIED MATERIALS & INTERFACES

Research Article

www.acsami.org

Unusual $Fe(CN)_6^{3-/4-}$ Capture Induced by Synergic Effect of Electropolymeric Cationic Surfactant and Graphene: Characterization and Biosensing Application

Sheng-Yuan Deng,[†] Tao Zhang,[‡] Dan Shan,*[,†,‡] Xiao-Yan Wu,[†] Yan-Zhi Dou,[‡] Serge Cosnier,[§] and Xue-Ji Zhang[†]

[†]School of Environmental and Biological Engineering, Nanjing University of Science and Technology, Nanjing 210094, China

[‡]School of Chemistry & Chemical Engineering, Yangzhou University, Yangzhou 225002, China

[§]Département de Chimie Moléculaire UMR-5250, ICMG FR-2607, CNRS Université Joseph Fourier, BP-53, 38041 Grenoble, France

Supporting Information

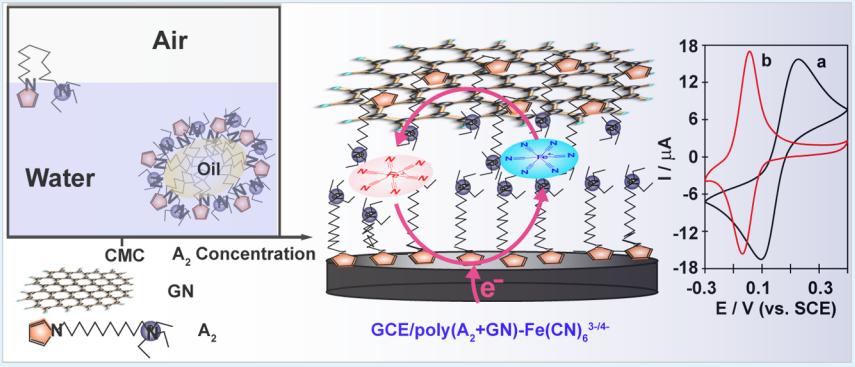

ABSTRACT: Herein, a special microheterogeneous system for $Fe(CN)_6^{3-/4-}$ capture was constructed based on graphene (GN) and the electropolymeric cationic surfactant, an amphiphilic pyrrole derivative, (11-pyrrolyl-1-yl-undecyl) triethylammonium tetrafluoroborate (A_2). The morphology of the system was characterized by scanning electron microscope. The redox properties of the entrapped $Fe(CN)_6^{3-/4-}$ were investigated by cyclic voltammetry and UV−visible spectrometry. The entrapped $Fe(CN)_6^{3-/4-}$ exhibited highly electroactive with stable and symmetrical cyclic voltammetric signal. A dramatic negative shift in the half wave potential can be obtained due to the unusual $Fe(CN)_6^{3-/4-}$ partitioning in in this microheterogeneous system based on poly(A_2+GN). Finally, the entrapped $Fe(CN)_6^{3-/4-}$ was applied in the construction of the enhanced biosensors to hydrogen peroxide and sulfide.

KEYWORDS: *amphiphilic pyrrole derivative, graphene, $Fe(CN)_6^{3-/4-}$ partitioning, sulfide, inhibition*

1. INTRODUCTION

Because of their simplicity and convenience, biosensors have obtained the boomed development for the desire of rapid detection and monitoring in clinical and food diagnostics and in environmental and biodefense.[1] Creating efficient electronic communications between the immobilized enzyme and the electrode surface is always important for the further development of biosensors. Utilization of electrochemical polymers and redox mediators are promising approaches.[2,3]

The electropolymerization technique and electropolymeric materials have exhibited prominent advantages, including low cost, flexible deposition on multiple substrates, wide molecular candidates, and the capability to incorporate or graft other materials for physiochemical modifications to realize versatile functions.[1] As it is well-known that pyrrole can be electrochemically polymerized, polypyrrole has been frequently used in electrocatalysis and biosensing because of its high electrical conductivity, environmental stability, and biocompatibility.[4] The pyrrole derivatives with wide variety of functional groups can be obtained via chemical synthesis. Thus, the conductivity of the electrogenerated polymers, their doping−dedoping process, the incorporation of stabilizers and their chemical functionalizations have been widely applied to provide a better electrochemical transduction and microenvironment of biological system.[5−7]

Surfactants are able to modify and control the properties of electrode surfaces owing to the two important properties of surfactants viz., adsorption at interface and aggregation into supramolecular structures.[8,9] (11-pyrrolyl-1-yl-undecyl) triethylammonium tetrafluoroborate is a kind of synthesized amphiphilic pyrrol denoted herein as A_2, which behaves the properties of a cationic surfactant.[6] Above a critical micelle

Received: September 6, 2014
Accepted: November 19, 2014
Published: November 19, 2014

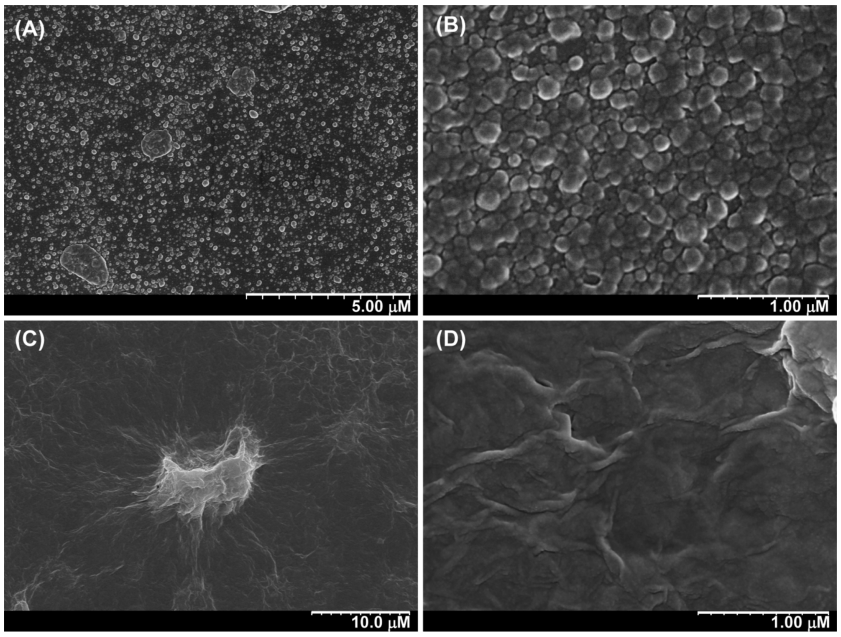

Figure 1. SEM images for (A, B) GCE/polyA$_2$ and (C, D) GCE/poly(A$_2$+GN).

concentration (CMC), A$_2$ micelles can be formed from soluble surfactants, which possess regions of hydrophilic and hydrophobic character. Based on this interesting information, A$_2$ micelles solution was used to construct a special microheterogeneous system incorporated with graphene (GN) by electropolymerization. GN has been considered as a "rising-star" material and has been used as labels for biosensing.[10,11] This system is expected to stably adsorb redox mediator $Fe(CN)_6^{3-/4-}$ through the synergic effect of electrostatic and $\pi-\pi$ interactions. The electrochemical behavior of the entrapped $Fe(CN)_6^{3-/4-}$ was investigated and its biosensing application was also evaluated.

2. EXPERIMENTAL SECTION

2.1. Reagents and Materials. Horseradish peroxidase (HRP) (EC 1.11.1.7, type II, 150U mg^{-1}) was purchased from Amresco. (11-Pyrrolyl-1-yl-undecyl) triethylammonium tetrafluoroborate (A$_2$) was synthesized according to the previously described protocol.[12] Graphene (GN) was prepared based on the chemical method.[13]All other chemicals were of analytical grade and used without further purification. Double-distilled water was used throughout the experiment. Phosphate buffer solution (PBS) was 0.1 M K_2HPO_4 and KH_2PO_4 and its pH was adjusted with H_3PO_4 or KOH solutions. H_2O_2 was freshly prepared before being used.

2.2. Measurements and Apparatus. A CHI 660D electrochemical workstation (CH Instrument) was used for cyclic voltammetry (CV) and amperometric measurements. All electrochemical studies were performed with a conventional three electrode system. A saturated calomel electrode (SCE) and a Pt wire electrode were used as reference and counter electrodes, respectively. All the potentials mentioned below are relative to SCE. The working electrode was a glassy carbon electrode (GCE) (diameter 3 mm). The working electrode was polished carefully with 0.05 μm alumina particles on silk followed by rinsing with distilled water and dried in air before use. UV–vis absorption spectra were collected using UV-2550 PC UV–visible spectrometer (Shimadzu, Japan). The morphology of the modified electrodes was investigated with a XL-30E scanning electron microscope (SEM). X-ray photoelectron spectra (XPS) were examined on a K-Alpha X-ray photoelectron spectrometer (Thermo Fisher Scientific Co., U.S.A.).

2.3. Preparation of PolyA$_2$ and PolyA$_2$/GA Modified Electrodes. The pyrrole-tethered cationic surfactant A$_2$ was dispersed in deionized water under sonication with a concentration of 8 mM. GN was dissolved in DMF with a concentration of 0.1 mg mL^{-1}. Initially, 10 μL of A$_2$ colloid solution was spread on the surface of clean GCE and was dried in ambient condition. This electrode was denoted as GCE/A$_2$. Second, 10 μL of GN was spread on the surface of GCE/A$_2$ and dried in ambient condition. The obtained electrode was denoted as GCE/A$_2$/GN. Finally, as-prepared GCE/A$_2$ and GCE/A$_2$/GN were transferred into an electrochemical cell containing an aqueous 0.1 M $LiClO_4$ and were electropolymerized by cyclic voltammetry between 0 to 0.9 V for 50 cycles at a scan rate of 50 mV s^{-1}, respectively, to obtain GCE/polyA$_2$ and GCE/poly(A$_2$+GN).

2.4. Preparation of GCE/poly(A$_2$+GN)-Fe(CN)$_6^{3-/4-}$. GCE/poly(A$_2$+GN) was dipped into 0.1 M PBS (pH 7.0) containing 10 mM $K_3Fe(CN)_6/K_4Fe(CN)_6$ (1:1) and potential scanned between 0 to 0.9 V for 50 cycles at a scan rate of 50 mV s^{-1}. Subsequently, the modified electrode was washed thoroughly with double-distilled water. The modified electrode obtained above was denoted as GCE/poly(A$_2$+GN)-Fe(CN)$_6^{3-/4-}$.

2.5. Fabrication of H_2O_2 Sensor. A 1.0 wt % chitosan solution was prepared by dissolving chitosan flakes in 1.0 wt % acetic acid (HAc). HRP was dissolved in 1.0 wt % chitosan with a concentration of 4 mg mL^{-1}. Ten microliters of HRP was dropped onto the surface of GCE/poly(A$_2$+GN)-Fe(CN)$_6^{3-/4-}$ and dried at room temperature.

2.6. Inhibitive Measurement Procedure. The inhibitive measurement followed our previous work:[14−16] As above, the prepared HRP-based electrode was dipped into a stirred PBS (pH 7.0) for a certain time until a stable baseline was achieved. The initial response current (I_1) of the bioelectrode to 0.8 M H_2O_2 was measured. When I_1 reached a steady state, we determined that the response current decreased (ΔI) because of the presence of sulfide. The degree of inhibition (inhibition %) is then calculated according to the equation generally used[14−16]

$$\text{inhibition}\% = \frac{\Delta I}{I_1}100$$

3. RESULTS AND DISCUSSION

3.1. XPS for the Synthesized Graphene. XPS measurement was performed to confirm the surface chemical composition of the synthesized graphene. The XPS survey

scan of graphene nanosheets shows distinct C 1s, N 1s, and O 1s peaks (see Figure S1 in the Supporting Information) with their corresponding relative atomic concentration of 91.70, 1.61, and 6.69 from elemental analysis. Such low O/C ratio of 7.3% indicated a well-preserved π-conjugated backbone with a few O-species at edge planes plus N adsorbates. The C−C peak at 284.8 eV become dominant in the C 1s XPS spectrum of GN (see Figure S2 in the Supporting Information), whereas three lesser deconvoluted peaks emerged assigned to C−O at 287.1 eV, C═O at 288.5 eV, and O−C═O at 289.6 eV, respectively, which further demonstrated that the primary bonding of C in GN contribute to the fast electron shuttling over the fabricated heterostructure.

3.2. Morphology. Morphological observation was taken by SEM. Figure 1 displays the micrographs of polyA$_2$ and poly(A$_2$+GN) films electrogenerated on the surface of GCE with different magnification. The present analysis reveals a clear morphological difference. The film of polyA$_2$ consists of compact and irregular micelle nanoparticles (Figure 1A, B), the size of which varies from 50 to 200 nm. As for poly(A$_2$+GN), the inherent wrinkled GN sheet appeared (Figure 1C, D, which shrinked dramatically during the electropolymerization process (Figure 1C). Because of $\pi-\pi$ interactions between aromatic pyrrole end-tail group and GN, the electropolymerized A$_2$ may be formed inner side of GN. Thus, the shrinked phenomenon can be observed.

The chemical structure of A$_2$ is illustrated in Figure 2. In view of its moderate polarity, the pyrrole substituent in A$_2$ could

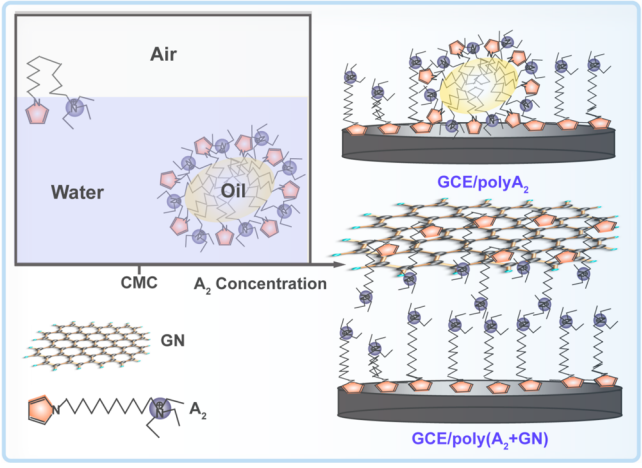

Figure 2. Schematic illustrations for chemical structure of A$_2$, A$_2$ conformation at the air−water interface, micelle structures, the proposed microstructure of GCE/polyA$_2$ and GCE/poly(A$_2$+GN).

behave as a polar terminal.[17] Thus, A$_2$ can be regarded as a sort of dipolar surfactants. It could be anticipated that the hydrophilic pyrrolic group concentrated at the air/water interface, prohibiting the folding of aliphatic chain into loop as depicted in Figure 2. Give the colloidal solution of A$_2$ utilized in this work slightly above its critical micelle concentration (CMC) of 5 ± 1 mM,[18] individually separated micelles with nonpolar interior and polar shell were formed and emerged as exhibited in Figure 1A. The resulting proximal A$_2$ could be electrochemically oxidized into soluble conducting oligomers. Meanwhile, the pyrrolyl moiety of A$_2$ monomer shows strong affinity with the basal plane of GN via π-stackingafter the introduction of GN/DMF solution. An integrated architecture of poly(A$_2$+GN) was finally achieved by this facile electrochemical polymerization.

3.3. Cyclic Voltammetric Response. The electrochemical behavior of $Fe(CN)_6^{3-/4-}$ captured in poly(A$_2$+GN) system was investigated by CVs as shown in Figure 3. At bare GCE

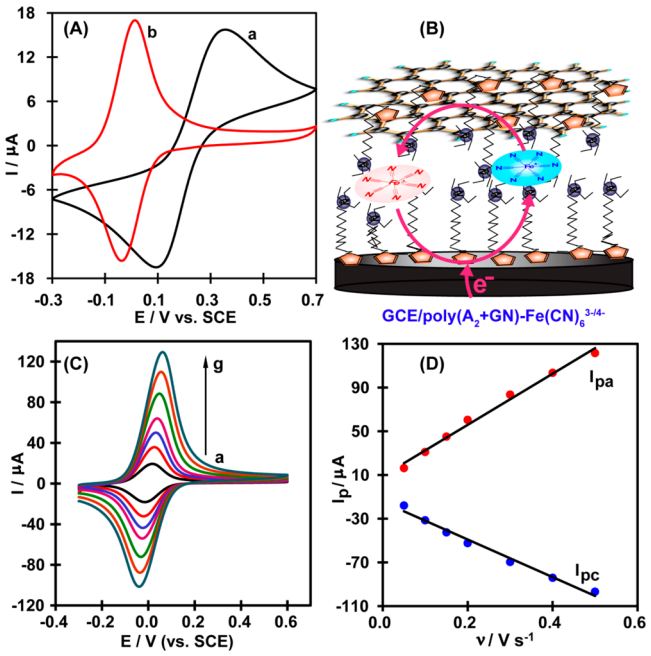

Figure 3. (A) Cyclic voltammograms recorded for (a) GCE in 0.1 M PBS (pH 7.0) containing 10 mM $K_3Fe(CN)_6/K_4Fe(CN)_6$ (1:1) and (b) GCE/poly(A$_2$+GN)-$Fe(CN)_6^{3-/4-}$ in 0.1 M PBS (pH 7.0), at scan rate of 50 mV s^{-1}. (B) Schematic representation of redox $Fe(CN)_6^{3-/4-}$ captured in the integrated poly(A$_2$+GN) system. (C) Cyclic voltammograms of GCE/poly(A$_2$+GN)-$Fe(CN)_6^{3-/4-}$ in 0.1 M PBS (pH 7.0) at various scan rates. The scan rate from inner to outer is (a) 50, (b) 100, (c) 150, (d) 200, (e) 300, (f) 400, and (g) 500 mV s^{-1} (from inner to outer). (D) Plots of anodic and cathodic peak currents vs scan rates.

(Figure 3A, curve a), $Fe(CN)_6^{3-/4-}$ exhibits a pair of redox peaks with the anodic peak potential (E_{pa}) at 333 mV and the cathodic peak potential (E_{pc}) at 108 mV. The peak-to-peak separation (ΔE_p = 225 mV) approximates the formal potential (E^{Φ}, the midpoint of E_{pa} and E_{pc}) of around 220 mV, and the ratio of corresponding peak currents (I_{pa}/I_{pc}) is 0.93, which bear the characteristics of a quasi-reversible process. Remarkably, for the $Fe(CN)_6^{3-/4-}$ entrapped in poly(A$_2$+GN) (Figure 3A, curve b), both E_{pa} and E_{pc} shifted negatively by 329 and 134 mV, respectively. Their peak-to-peak separation is calculated to be 30 mV plus the I_{pa}/I_{pc} of about 1 and E^{Φ} = 11 mV, comparatively shifted toward zero by 231 mV. The dramatically reduced ΔE_p demonstrates a fast electron transfer promoted by the microheterogeneous system of poly(A$_2$+GN), which derives from the partitioning of electroactive probes in microheterogeneous systems like $Fe(CN)_6^{3-/4-}$ at ionic liquid modified electrode.[19,20] Furthermore, the CVs of GCE/poly(A$_2$+GN)-$Fe(CN)_6^{3-/4-}$ reveal well-defined symmetric peaks at different scan rates (υ); meanwhile, both I_{pa} and I_{pc} increase as υ grows from 50 up to 500 mV s^{-1} (Figure 3C). The peak currents vary linearly with υ (Figure 3D), whose linear regression equations are I_{pa} (μA) = 233.89 mV s^{-1} + 9.1209 (R^2 = 0.9907, n = 7) and I_{pc} (μA) = −172.13 mV s^{-1} − 14.583 (R^2 = 0.9856, n = 7), respectively. This suggests that surface-

dx.doi.org/10.1021/am506057d | ACS Appl. Mater. Interfaces 2014, 6, 21161−21166

controlled mechanism dominates the electron transfer process for $Fe(CN)_6^{3-/4-}$ confined in the microstructure of poly-(A_2+GN). According to $I_p = n^2F\upsilon A\Gamma/4RT$,[21] where Γ represents the average surface coverage of redox substance (mol cm^{-2}), A designates the electrode area (0.07 cm^2), and n, F, R, and T also have their established meanings. Hence, Γ is estimated to be 3.56×10^{-9} mol cm^{-2}. Additionally, the presence of $\pi-\pi$ interaction between the incorporated GN sheet and −CN greatly strengthened the entrapment of $Fe(CN)_6^{3-/4-}$ within the microheterogeneous system of poly(A_2+GN); on the other hand, $Fe(CN)_6^{3-}$ and $Fe(CN)_6^{4-}$ as soluble multicharged anions could strongly associate with the polymerized cationic surfactant polyA_2 in the microheterogeneous system (Figure 3B), which overall lead to an exceptionally stable electrochemical signal: both the peak current and the potential remain nearly unchanged even after 100 cycles (data not shown).

3.4. UV−Vis Spectra. Figure 4 shows the spectra of 1 mM $Fe(CN)_6^{3-/4-}$ (Figure 4, curve a) and the captured Fe-

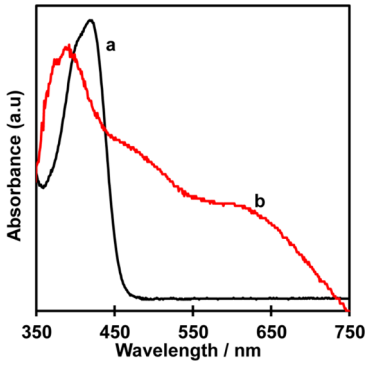

Figure 4. UV−vis spectra for (a) 1 mM $Fe(CN)_6^{3-/4-}$ and (b) the film of poly(A_2+GN)-$Fe(CN)_6^{3-/4-}$ formed on ITO glass.

$(CN)_6^{3-/4-}$ on poly(A_2+GN) modified ITO glass (Figure 4, curve b). As reported in the literature,[22,23] $Fe(CN)_6^{3-/4-}$ features an absorption band at around 413 nm attributed to the charge transfer from Fe^{2+} to −CN (Figure 4, curve a). As for poly(A_2+GN)-$Fe(CN)_6^{3-/4-}$, the absorption band blue-shifted to 385 nm compared with that of mere $Fe(CN)_6^{3-/4-}$ (Figure 4, curve b). This suggests a strong association between positive-charged polyA_2 and the cyanide complex, affecting the intrinsic property of $Fe(CN)_6^{3-/4-}$. In addition, absorption due to $\pi \rightarrow \pi^*$ transition is reported to appear in the visible region at wavelengths of 620 nm Davydov splitting (Q-band).[24] It indicates that the synergic effect of electropolymeric cationic surfactant and GN can realize the stable capture of redox probe of $Fe(CN)_6^{3-/4-}$.

3.5. H_2O_2 Sensor. HRP was immobilized on the surface of GCE/poly(A_2+GN)-$Fe(CN)_6^{3-/4-}$ and the electrocatalytic activity to H_2O_2 was examined using cyclic voltammetry (Figure 5, inset A). In the absence of H_2O_2, the enzyme electrode presents the cyclic voltammogram corresponding to the underlying GCE/poly(A_2+GN)-$Fe(CN)_6^{3-/4-}$ (inset A, curve a). When H_2O_2 was added to the buffer solution, an increase in I_{pc} was observed with the decrease of I_{pa} at around 0 V (inset B, curve b). Such phenomenon unambiguously reveals an electrocatalytic reduction of H_2O_2 by the GCE/poly-(A_2+GN)-$Fe(CN)_6^{3-/4-}$/HRP.

The electrocatalytic reduction of hydrogen peroxide at the enzyme electrode was also studied by amperometry, which is

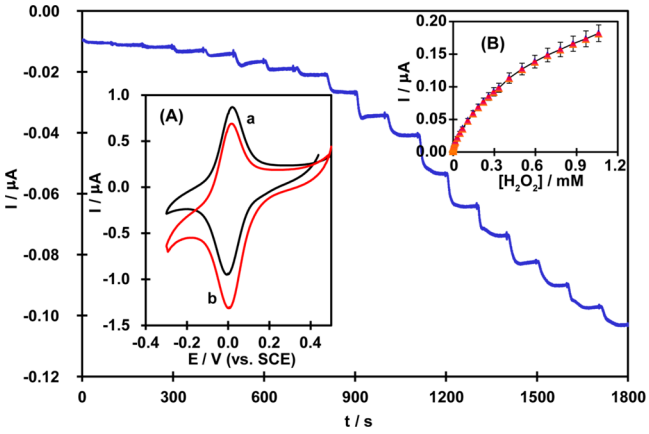

Figure 5. Typical steady-state response of the proposed HRP based-electrode on successive injection of H_2O_2 into 10 mL of stirring 0.1 M PBS (pH 7.0), applied potential: −0.05 V, vs SCE. Inset A: Cyclic voltammograms for the proposed HRP electrode recorded in 0.1 M PBS (pH 7.0) in (a) the absence and (b) presence of 1 mM H_2O_2, scan rate: 5 mV s^{-1}. Inset B: The corresponding calibration curve of the proposed HRP based-electrode to H_2O_2.

one of the most widely employed techniques for biosensor. Figure 5 displays the amperometric response of different concentrations of H_2O_2 at GCE/poly(A_2+GN)-$Fe(CN)_6^{3-/4-}$/HRP in the detection solution. The applied potential was kept at −0.05 V. Upon the addition of aliquoted H_2O_2, the reduction current dived to reach a plateau. The proposed HRP-based-electrode could achieve 95% of the steady-state current within 10 s. The corresponding calibration curve was shown inset B of Figure 5. The response to H_2O_2 is linear in the range from 5.6×10^{-6} to 5.9×10^{-4} M and detection limit down to 1.9×10^{-6} M at a signal-to-noise ratio of 3. The detection limit is comparable to those obtained at nano-$CaCO_3$−HRP/polyBCB/SWCNTs/GCE[25] (1.0×10^{-6}) and GC/poly(GMA-*co*-VFc)/HRP[26] (2.6×10^{-6}), and lower than that obtained at HRP/polyBCB/GCE[27] (4.2×10^{-6}). Unfortunately, the sensitivity is calculated to be 5.99 mA M^{-1} cm^{-2}, which is not so satisfactory. It may be attributed the rough preparation of the proposed HRP electrode simply by casting HRP solution onto the surface of mediated electroactive electrode. Nevertheless, the sensitivity could be further enhanced by coimmobilization of HRP and mediator at the same phase.

3.6. Inhibitory Effect of Sulfide. Sulfide contamination in water causes serious environmental problems and presents a danger to human health. Therefore, sulfide content is a very important pollution index for water.[28] Because sulfides are able to attack the heme group, causing much more severe inadivation by blocking the active site of HRP.[24] Several biosensors for inhibitive determination of sulfide have been developed.[3,14,29−33]For further comprehensive studies of the biocatalytic behavior of the proposed HRP based electrode, we evaluated the inhibitory effect of sulfide. Curve a in Figure 6 demonstrates the time-dependent response of the proposed HRP-based electrode to Na_2S. The left part displays the amperometric response to 0.8 mM H_2O_2. The right part illustrates the response decrease due to the presence of Na_2S in the H_2O_2 solution, implying that Na_2S inhibits the activity of the immobilized HRP. For each injection, a dramatically decreased current can be observed. The response time of the proposed HRP-bioelectrode to Na_2S is less than 5 s. This response time is shorter than the amount of 43 and 65 s

dx.doi.org/10.1021/am506057d | ACS Appl. Mater. Interfaces 2014, 6, 21161−21166

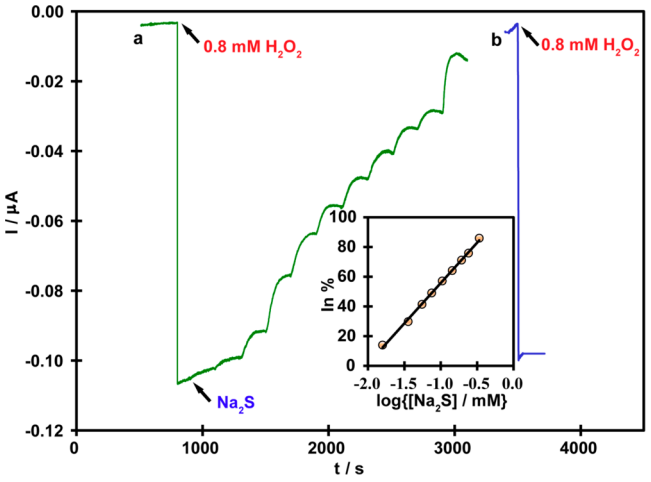

Figure 6. Reversibility of inhibition of sulfide to the proposed HRP based-electrode. (a) Typical current−time recordings at the proposed HRP based-electrode upon increasing various concentrations of Na_2S, applied potential, −0.05 V; 0.1 M PBS containing 0.8 mM H_2O_2. (b) Another response of the same HRP based-electrode to 0.8 mM H_2O_2 after contacting with Na_2S and rinsing with PBS simply. Inset: Linearization of the calibration curve.

obtained at CIP/chitosan/SPE[31] and Con A/HRP bilayer sensor.[32]The inhibition (In%) increases with the increase of Na_2S concentration. A typical inhibition calibration curve for the determination of Na_2S is displayed in inset of Figure 6. There is a linear dependence between the logarithm of the Na_2S concentration and the inhibition (%), when the concentration of H_2O_2 being fixed at 0.8 mM. The linear range covers from 1.6×10^{-5} to $\sim 3.4 \times 10^{-4}$ M with a slope of 54.3 (%/log{[Na_2S]/mM}) and a correlation coefficient of 0.998 (n = 10). The detection limit is found to be 1.9×10^{-6} M based on 10% inhibition degree as a standard, considering the error of the measurement. The detection limit is much lower than that the value 8 μM reported by Zhao et al.[29] IC_{50}, i.e., the concentration of the inhibitor corresponding to 50% of the inhibition signal was calculated to be 0.1 mM. Furthermore, the initial response for H_2O_2, i.e., restoration of the enzyme activity, could be obtained again. The data indicates the response of the proposed HRP-based electrode to H_2O_2 retains 95.6% of its original response (Figure 6, curve b). This behavior suggests the inhibition of Na_2S is reversible. This makes it possible to use continuous measurement methodology for Na_2S assay.

4. CONCLUSION

Amphiphilic surfactant could be converted into conducting polymer films at carbon-based electrode by the adsorption of micelle solution via electrochemical oxidation. Meanwhile, GN can be firmly integrated with polyA$_2$ into microheterogeneous hierarchical scaffolds through facile electrochemical oxidation. The electroactive probe $Fe(CN)_6^{3-/4-}$ can further be partitioned into this system due to the synergistic interactions of both electrostatic and π-stacking. Ascribed to the promoted conductivity and large specific surface area of the modified electrode, the entrapped $Fe(CN)_6^{3-/4-}$ has emerged as having exceptionally efficient electrocatalytic capability toward the reduction of H_2O_2, facilitating the fabrication of a highly sensitive sensor to inhibitive determination of sulfides.

ASSOCIATED CONTENT

Supporting Information

XPS survey scan and C 1s spectra of GN. This material is available free of charge via the Internet at http://pubs.acs.org.

AUTHOR INFORMATION

Corresponding Author

*E-mail: danshan@njust.edu.cn or danshan@yzu.edu.cn.

Notes

The authors declare no competing financial interest.

ACKNOWLEDGMENTS

This research was supported by National Natural Science Foundation of China (Grants 21175114, 21305067), the Natural Science Foundation of Jiangsu Province (BK2011441, 20130754), PhD Fund of MOE for Young Teachers (0133219120019), Qing Lan project of Jiangsu Province, NJUST Research Dounding (2012ZDJH009) and the Fundamental Research Funds for the Central Universities (30920130112012).

REFERENCES

(1) Cosnier, S.; Holzinger, M. Electrosynthesized Polymers for Biosensing. *Chem. Soc. Rev.* **2011**, *40*, 2146−2156.
(2) Le Goff, A.; Holzinger, M.; Cosnier, S. Enzymatic Biosensors Based on SWCNTs-Conducting Polymer Electrodes. *Analyst.* **2011**, *136*, 1279−1287.
(3) Cosnier, S. Biosensors Based on Electropolymerized Films: New Trends. *Anal. Bioanalchem.* **2003**, *37*, 507−520.
(4) Lalaoui, N.; Elouarzaki, K.; Le Goff, A.; Holzinger, M.; Cosnier, S. Efficient Direct Oxygen Reduction by Laccases Attached and Oriented on Pyrene-Functionalized Polypyrrole/Carbon Nanotube Electrodes. *Chem. Commun.* **2013**, *49*, 9281−9283.
(5) Xu, H.; Gorgy, K.; Gondran, C.; Le Goff, A.; Spinelli, N.; Lopez, C.; Defrancq, E.; Cosnier, S. Label-Free Impedimetric Thrombin Sensor Based on Poly(Pyrrole-Nitrilotriacetic Acid)-Aptamer Film. *Biosens. Bioelectron.* **2013**, *41*, 90−95.
(6) Cosnier, S.; Ionescu, R. E.; Holzinger, M. Aqueous Dispersions of SWCNTs Using Pyrrolic Surfactants for Electro-generation of Homogeneous Nanotube Composites, Application to the Design of an Amperometric Biosensor. *J. Mater. Chem.* **2008**, *18*, 5129−5133.
(7) Haddour, N.; Cosnier, S.; Gondran, C. Electrogeneration of Poly(pyrrole)-NTA Chelator Film for a Reversible Oriented Immobilization of Histidine-Tagged Proteins. *J. Am. Chem. Soc.* **2005**, *127*, 5752−5753.
(8) Zhu, L. L.; Cao, Y. H.; Cao, G. Q. Electrochemical Sensor Based on Magnetic Molecularly Imprinted Nanoparticles at Surfactant Modified Magnetic Electrode for Determination of Bisphenol. *Biosens. Bioelectron.* **2014**, *54*, 258−261.
(9) Pajootan, E.; Arami, M. Structural and Electrochemical Characterization of Carbon Electrode Modified by Multi-Walled Carbon Nanotubes and Surfactant. *Electrochim. Acta* **2013**, *112*, 505−514.
(10) Loo, A. H.; Bonanni, A.; Pumera, M. Inherently Electroactive Graphene Oxide Nanoplatelets as Labels for Specific Protein-Target Recognition. *Nanoscale* **2013**, *5*, 7844−7848.
(11) Bonanni, A.; Chua, C. K.; Zhao, G. J.; Sofer, Z.; Pumera, M. Inherently Electroactive Graphene Oxide Nanoplatelets as Labels for Single Nucleotide Polymorphism. *ACS Nano* **2012**, *6*, 8546−8551.
(12) Ionescu, R. E.; Cosnier, S.; Marks, R. S. Protease Amperometric Sensor. *Anal. Chem.* **2006**, *78*, 6327−6331.
(13) Chen, G. H.; Weng, W. G.; Wu, D. J.; Wu, C. L.; Lu, J. R.; Wang, P. P.; Chen, X. F. Preparation and Characterization of Graphite Nanosheets from Ultrasonic Powdering Technique. *Carbon* **2004**, *42*, 753−759.

(14) Shan, S.; Li, Q. B.; Ding, S. N.; Xu, J. Q.; Cosnier, S.; Xue, H. G. Reagentless Biosensor for Hydrogen Peroxide Based on Self-Assembled Films of Horseradish Peroxidase/Laponite/Chitosan and the Primary Investigation on the Inhibitory Effect by Sulfide. *Biosens. Bioelectron.* **2010**, *26*, 536−541.
(15) Shan, D.; Mousty, C.; Cosnier, S. Subnanomolar Cyanide Detection at Polyphenol Oxidase/Clay Biosensors. *Anal. Chem.* **2004**, *76*, 178−183.
(16) Shan, S.; Cosnier, S.; Mousty, C. HRP/[Zn-Cr-ABTS] Redox Clay-Based Biosensor: Design and Optimization for Cyanide Detection. *Biosens. Bioelectron.* **2004**, *20*, 390−396.
(17) Chevalier, Y. New Surfactants: New Chemical Functions and Molecular Architectures. *Curr. Opin. Colloid Interface Sci.* **2002**, *7*, 3−11.
(18) Berlot, I.; Chevalier, Y.; Labbé, P.; Moutet, J. C. Interfacial and Micellar Behavior of Pyrrole-Containing Cationic Surfactants. *Langmuir* **2001**, *17*, 2639−2646.
(19) Wadhawan, J. D.; Schröder, U.; Neudeck, A.; Wilkins, S. J.; Compton, R. G.; Marken, F.; Consorti, C. S. Ionic Liquid Modified Electrodes. Unusual Partitioning and Diffusion Effects of $Fe(CN)_6^{4-/3-}$ in Droplet and Thin Layer Deposits of 1-Methyl-3-(2,6-(S)-Dimethylocten-2-yl)-Imidazolium Tetrafluoroborate. *J. Electroanal. Chem.* **2000**, *493*, 75−83.
(20) Myers, S. A.; Mackay, R. A.; Brajter-Toth, A. Solution Microstructure and Electrochemical Reactivity. Effect of Probe Partitioning on Electrochemical Formal Potentials in Microheterogeneous Solutions. *Anal. Chem.* **1993**, *65*, 3447−3453.
(21) Laviron, E. The Use of Linear Potential Sweep Voltammetry and of A.C. Voltammetry for the Study of the Surface Electrochemical Reaction of Strongly Adsorbed Systems and of Redox Modified Electrodes. *J. Electroanal. Chem.* **1979**, *100*, 263−270.
(22) Hwang, H. J.; Lu, Y. Spectroscopic Evidence for Interactions Between Hexacyanoiron(II/III) and an Engineered Purple Cu_A Azurin. *J. Inorg. Biochem.* **2004**, *98*, 797−802.
(23) Ali, I. O.; Salama, T. M.; Thabet, M. S.; El-Nasser, K. S.; Hassan, A. M. Encapsulation of Ferro- and Ferricyanide Complexes Inside ZSM-5 Zeolite Synthesized from Rice Straw: Implications for Synthesis of Prussian Blue Pigment. *Mater. Chem. Phys.* **2013**, *140*, 81−88.
(24) Padam, N.; Joshi, A.; Singh, A.; Deshpande, S. K.; Aswal, D. K.; Gupta, S. K.; Yakhmi, J. V. NO_2 Sensors with Room Temperature Operation and Long Term Stability Using Copper Phthalocyanine Thin Films. *Sens. Actuators, B* **2009**, *143*, 246−252.
(25) Chen, M.; Xu, J. Q.; Ding, S. N.; Shan, D.; Xue, H. G.; Cosnier, S.; Holzinger, M. Poly(Brilliant Cresyl Blue) Electrogenerated on Single-Walled Carbon Nanotubes Modified Electrode and Its Application in Mediated Biosensing System. *Sens. Actuators, B* **2011**, *152*, 14−20.
(26) Şenel, M.; Çevik, E.; Abasıyanık, M. F. Amperometric Hydrogen Peroxide Biosensor Based on Covalent Immobilization of Horseradish Peroxidase on Ferrocene Containing Polymeric Mediator. *Sens. Actuators, B* **2010**, *145*, 444−450.
(27) Ghica, M. E.; Brett, C. M. A. Poly(Brilliant Cresyl Blue) Modified Glassy Carbon Electrodes: Electrosynthesis, Characterization and Application in Biosensors. *J. Electroanal. Chem.* **2009**, *629*, 35−42.
(28) Puacz, W.; Szahun, W.; Linke, K. Catalytic Determination of Sulfide in Blood. *Analyst* **1995**, *120*, 939−941.
(29) Zhao, J. G.; Henkens, R. W.; Crumbliss, A. L. Mediator-Free Amperometric Determination of Toxic Substances Based on Their Inhibition of Immobilized Horseradish Peroxidase. *Biotechnol. Prog.* **1996**, *12*, 703−708.
(30) Yang, Y. H.; Yang, M. H.; Wang, H.; Jiang, J. H.; Shen, G. L.; Yu, R. Q. An Amperometric Horseradish Peroxidase Inhibition Biosensor Based on a Cysteamine Self-Assembled Monolayer for the Determination of Sulfides. *Sens. Actuators, B* **2004**, *102*, 162−168.
(31) Savizi, I. S. P.; Kariminia, H. R.; Ghadiri, M.; Azad, R. R. Amperometric Sulfide Detection Using Coprinus Cinereus Peroxidase Immobilized on Screen Printed Electrode in an Enzyme Inhibition Based Biosensor. *Biosens. Bioelectron.* **2012**, *35*, 297−301.
(32) Liu, L. J.; Chen, Z. C.; Yang, S. M.; Jin, X.; Lin, X. F. A Novel Inhibition Biosensor Constructed by Layer-by-Layer Technique Based on Biospecific Affinity for the Determination of Sulfide. *Sens. Actuators, B* **2008**, *129*, 218−224.
(33) Poor, N. Z. M.; Baniasadi, L.; Omidi, M.; Amoabediny, G.; Yazdian, F.; Attar, H.; Heydarzadeh, A.; Zarami, A. S. H.; Sheikhha, M. H. An Inhibitory Enzyme Electrode for Hydrogen Sulfide Detection. *Enzyme. Microb. Technol.* **2014**, *63*, 7−12.